Development of nanoparticle catalysts and total internal reflection (TIR) Raman spectroscopy for improved understanding of heterogeneous catalysis

LAURA MARIA BINGHAM

Chapter 5. *In situ* studies of ethylene hydrogenation using total internal reflection (TIR) Raman spectroscopy

5.1. Ethylene hydrogenation

In Chapter 3 proof of concept for TIR Raman spectroscopy was undertaken showing the ability to detect capping agents present within nanoparticle monolayers upon a silica hemisphere. The work within this chapter extends this study moving on to the use of TIR Raman spectroscopy for the *in situ* study of ethylene hydrogenation. Ethylene hydrogenation was chosen as a system to investigate due to a number of considerations as discussed in Chapter 1, Section 1.6.1. The reaction had been widely investigated in the literature and so represented a relatively well understood example, making it a desirable starting point for our *in situ* catalytic studies *via* TIR Raman spectroscopy. One such example that was used as a starting point for the catalytic conditions adopted in this work was that of Cremer *et al*..[1] In their work, the hydrogenation of ethylene at platinum surfaces was investigated using sum frequency generation (SFG). The conditions used by the authors in terms of the partial pressures of the gas feeds were replicated within this work (Chapter 2, Section 2.2.6.1).

5.1.1. Calculation for variation of reaction conditions upon proportion of free and absorbed molecules probed

Some basic calculations were undertaken in order to estimate the rough influence of variation of reaction conditions and measurement parameters upon the proportion of absorbed versus free molecules probed, such as gas feed (partial pressure), temperature, laser angle and excitation wavelength. This is of interest as both free and absorbed molecules are capable of causing Raman scattering, although only those bound to the surface are of primary interest in this application (*i.e.* we want to probe at the catalytic interface only). A basic equation to describe the impact of experimental conditions upon this ratio can be formulated, as shown in Equation 5.1, by calculating the number of molecules probed at the surface over the area illuminated and multiplying by the intensity at the surface, I_0, then comparing this to the gas molecules probed and the intensity of the light, based on the exponential decay of the evenescent wave. The equation refers to molecule A which can be both adsorbed at the surface or present in the gas phase with the laser spot illuminated given by A_{spot}, and for the adsorbed species the intensity of light is in the surface layer is taken to be I_0. An ideal gas is assumed, and a number of absorbed molecules per unit area of 16 nm^{-2}.

$$Ratio = \frac{scattering\ due\ to\ absorbed\ species}{scattering\ due\ to\ gas\ phase} \qquad \textit{Equation 5.1}$$

$$= \frac{N_{abs} I_o}{\int_0^\infty \frac{N_{gas}}{z} I(z) dz} = \frac{A_{spot} 0.16\ nm^{-2} I_0}{\int_0^\infty \frac{p_A V}{K_b T z} I(z) dz}$$

$$= \frac{k_b T A_{spot} 0.16\ nm^{-2}.I_0}{p_A A_{spot} I_0 \int_0^\infty \exp(-\frac{z}{d}) dz}$$

$$= \frac{k_b T 0.16\ nm^{-2}}{p_A d}$$

Substituting standard experimental conditions (T=298 K, P=0.04 bar, θ=73°, λ=660 nm) into Equation 5.1 provides a ratio, and subsequently varying one parameter allows the impact of this parameter upon the ratio of molecules probed to be evaluated (Figure 5.1). Temperature variation has the smallest effect upon the ratio, displaying a low gradient straight line. This is desirable as heating of the sample is often necessary for studying catalytic applications. For partial pressure a dramatic variation is seen, with low partial pressures resulting in the probing of mainly adsorbed surface molecules, while high pressures correspond to the probing of predominantly gas phase molecules. This needs to be taken into consideration when selecting gas feed conditions. For θ variation the effect is again less severe, although lower angles result in the probing of more gas phase molecules and the converse is seen from the use of higher incident laser angles. The set 73° angle used sits intermediate of these two conditions, so would not be suspected to hamper sensing of the absorbed monolayer (Section 2.1.5.5) (Note: this ignores any sensitivity due to polarisation dependent or absorption geometry dependent effects that are also angle dependent). Finally, for the variation of λ, low values correspond to the desired probing of mainly absorbed molecules although at 660 nm a significant proportion of free molecules will be sensed. Although it is clearly desirable to operate in conditions that maximise the sensitivity to adsorbed species, this doesn't mean it is impossible to look at adsorbed species in the presence of gas phase molecules if the signals do not overlap, since adsorption typically also results in changes in vibrational energies and therefore a Raman shift of spectral features.

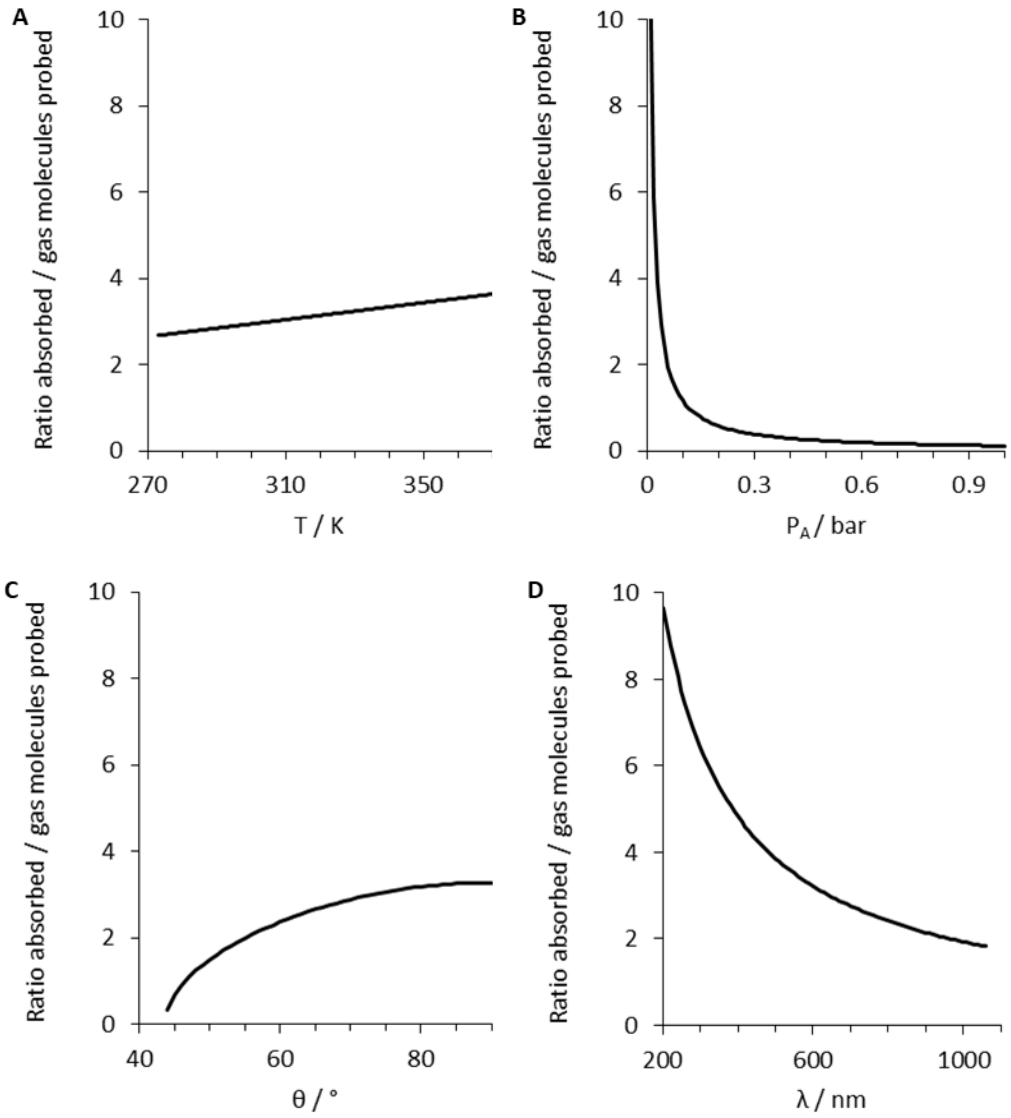

Figure 5.1. Graphs to demonstrate calculation of the effect upon the ratio of absorbed surface molecules to gas molecules probed for variation of the following parameters A) temperature (T) variation, B) pressure (P) variation, C) angle (ϑ) variation, D) wavelength (λ) variation. For each variable all other parameters were fixed to T=298 K, P=0.04 bar, ϑ=73°, λ=660 nm.

5.1.2. Ethylene hydrogenation studies over a platinum/polyvinylpyrrolidone nanoparticle (platinum/PVP np) catalyst

This work and that in Chapter 3 took place using the pre-existing setup (System 2) described in Section 2.2.4.2. This setup was not designed or otherwise optimised for the work being conducted, but used to deliver the best results possible within the constraints of the system. The catalyst studied was a monolayer sample of platinum/polyvinylpyrrolidone nanoparticles (platinum/PVP nps) supported by deposition upon a silica hemisphere. The deposited sample had been plasma cleaned for 2 min in order to provide a clean surface for both spectroscopy and catalysis. This time was selected on the basis of other nanoparticle

systems as seen in Chapter 3, and scanning electron microscopy (SEM) imaging of plasma cleaned platinum/PVP np samples.

Initial TIR Raman spectra collected in the presence of different gas mixtures are shown in Figure 5.2 and 5.3. Each spectra in which a controlled gas composition was present (Figures 5.2 and 5.3, spectra labelled 2 (helium), 3 (helium and hydrogen), and 4 (helium, hydrogen, and ethylene) displayed a corresponding increase in background intensity (this was consistent across all of the regions of interest) with bands appearing broad and displaying no clear correspondence to any features expected from the literature.[2] In order to remove this background the purity of the gas feed was investigated. The plastic tubing used to deliver the gas feed was replaced with metal tubing in order to prevent any possibility of leaching of contaminants from the plastic into the gas, and to allow for the tubing to be more readily cleaned (with propan-2-ol and compressed nitrogen). A zeolite adsorbent was also fitted to the hydrogen gas supply for the removal of any small level impurities present in the gas feed. Spectra taken after implementation of these procedures are given in Figures 5.4 and 5.5. For spectra in which gases were flowed across the hemisphere (Figures 5.4 and 5.5, spectra labelled 2 (helium), 3 (helium, and hydrogen), and 4 (helium, hydrogen, and ethylene)) a significant decrease was seen in the intensity of the background as compared to the spectra in Figures 5.2 and 5.3. This indicated success in the changes made and these changes would now be implemented as a standard procedure in all subsequent work. Even in the absence of these background peaks no other spectral features could be resolved. In Chapter 3 fluorescence had been seen for bulk Raman spectra of drop cast platinum/PVP nps, attributed to the capping agent. Fluorescence might therefore be expected to contribute to the inability to detect any spectral features for the platinum/PVP np sample in this case, and so switching to a nanoparticle system which did not display such high levels of fluorescence might be recommended. Although it should be noted that no such florescence had been seen for TIR spectra of monolayer platinum/PVP nps which was presumably due to the low particle concentration. TIR Raman spectra recorded for the platinum/PVP np samples both before and after plasma cleaning are given in the Appendix (Figures 5A.1 and 5A.2). Although no spectral features were identified prior to plasma cleaning, a reduced intensity of the silica bands was seen after plasma cleaning as compared to that seen before plasma cleaning, and would be suggestive of the removal of a surface bound species, assuming an acceptable comparable focus was obtained. This suggests inefficient removal of the capping agent prior to catalysis should not have prevented adsorption of molecules at the platinum surface.

In Chapter 3, spectra recorded for palladium/oleylamine nanoparticle (palladium/OAm np) samples (after the studies described above were performed) showed a number of features attributable to organic capping agents prior to plasma cleaning and spectra acquired after the plasma cleaning protocol demonstrated their successful removal. Platinum/oleylamine nanoparticles (platinum/OAm nps, for which no significant fluoresce had been detected) might therefore be expected to constitute a better nanoparticle system for TIR Raman *in situ* spectroscopic studies of ethylene hydrogenation are so were used in subsequent studies.

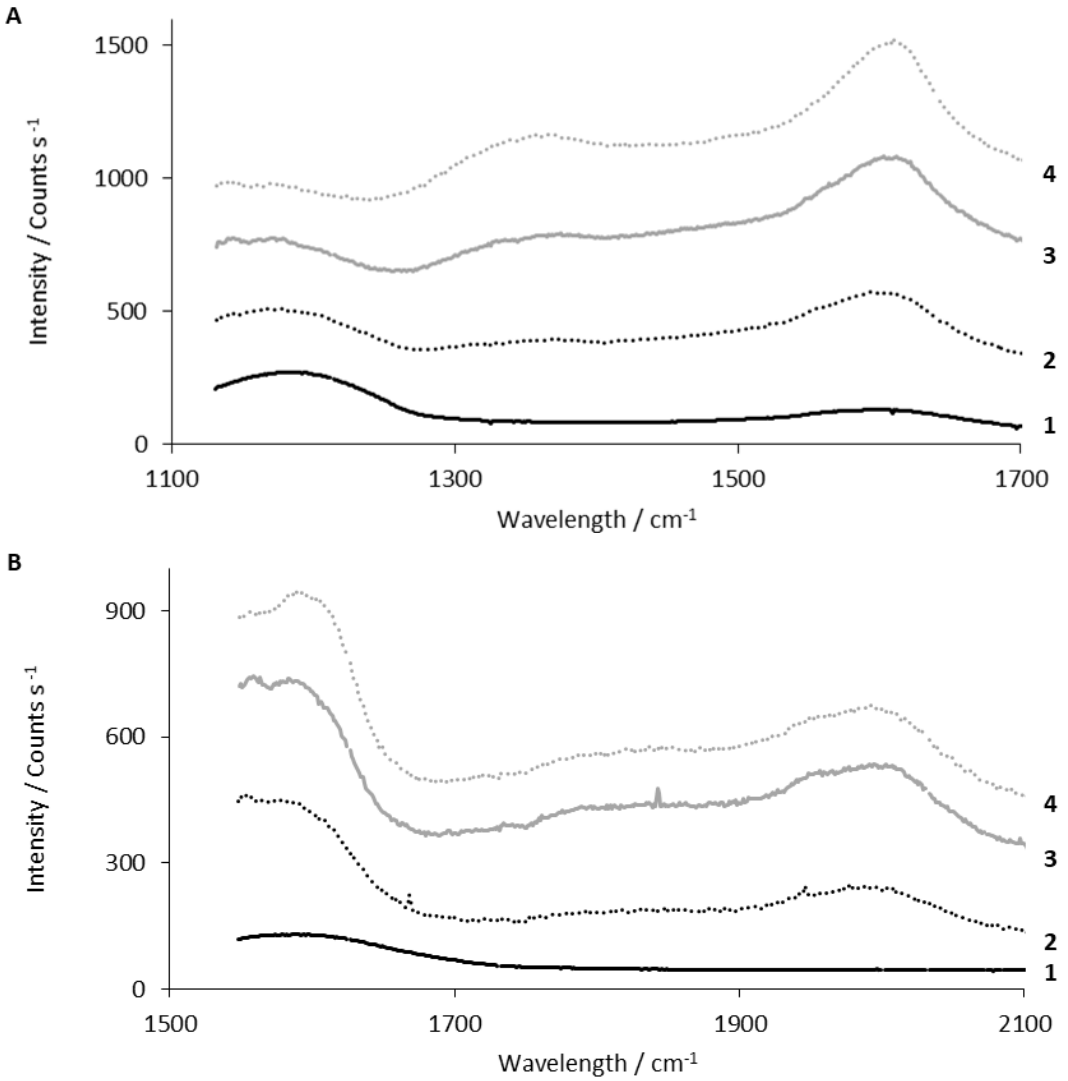

Figure 5.2. TIR Raman spectra of platinum/PVP nps Langmuir Blodgett (LB) deposited on a silica hemisphere and plasma cleaned for 2 min 1- with no gas flow, 2- with helium (0.82 bar) flowing through the cell, 3- with a mixture containing helium (0.82 bar), and hydrogen (0.13 bar) flowing through the cell, 4- with a mixture containing helium (0.82 bar), hydrogen (0.13 bar), ethylene (0.05 bar). Figures 5.2 A-B and 5.3 A show regions at which spectral features were expected on the basis of prior literature.[2] *Spectrum 1 was taken for a laser power of 600 mW with an exposure time of 5 s for 10 frames. Spectra 2 to 4 were taken for a laser power of 600 mW with an exposure time of 4 s for 10 frames. Spectra have been offset vertically for clarity. Single point data, attributed to stray electronic signals, have been removed as part of data processing. All spectra were collected with a 532 nm excitation wavelength.*

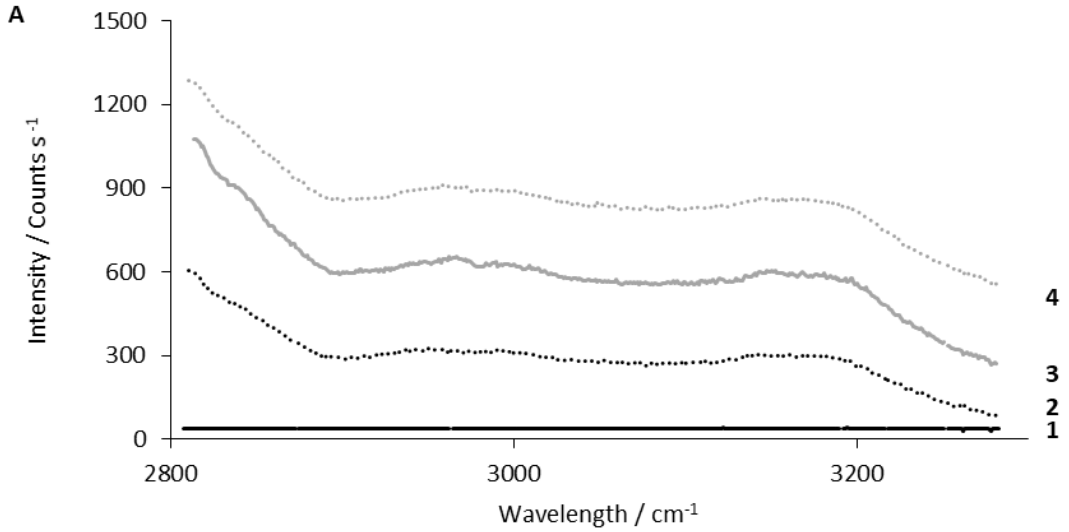

Figure 5.3. TIR Raman spectra of platinum/PVP nps Langmuir Blodgett (LB) deposited on a silica hemisphere and plasma cleaned for 2 min 1- with no gas flow, 2- with helium (0.82 bar) flowing through the cell, 3- with a mixture containing helium (0.82 bar), and hydrogen (0.13 bar) flowing through the cell, 4- with a mixture containing helium (0.82 bar), hydrogen (0.13 bar), ethylene (0.05 bar). Figures 5.2 A-B and 5.3 A show regions at which spectral features were expected on the basis of prior literature.[2] *Spectrum 1 was taken for a laser power of 600 mW with an exposure time of 5 s for 10 frames. Spectra 2 to 4 were taken for a laser power of 600 mW with an exposure time of 4 s for 10 frames. Spectra have been offset vertically for clarity. Single point data, attributed to stray electronic signals, have been removed as part of data processing. All spectra were collected with a 532 nm excitation wavelength.*

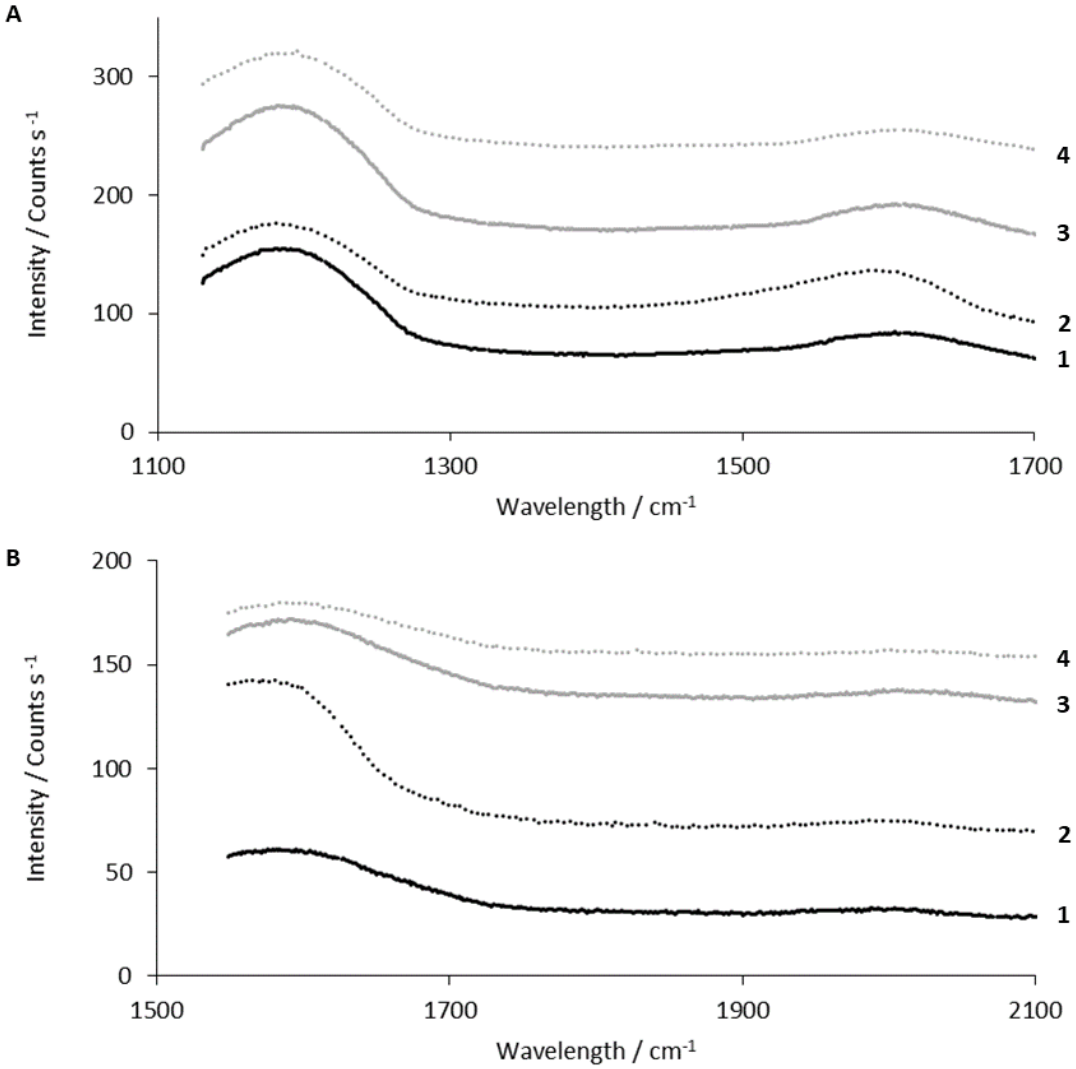

Figure 5.4. TIR Raman spectra of platinum/PVP nps LB deposited on a silica hemisphere and plasma cleaned for 2 min. Spectra were taken after replacement of the metal tubing, used to supply gas flow to the system, to nylon took place, as well as the addition of a zeolite adsorbent fitted to the hydrogen gas supply in order to remove any possible contamination. Figures 5.4 A-B and 5.5 A were taken with the following gas flow conditions 1- with no gas flow, 2- with helium (0.82 bar) flowing through the cell, 3- with a mixture containing helium (0.82 bar), and hydrogen (0.13 bar) flowing through the cell, 4- with a mixture containing helium (0.82 bar), hydrogen (0.13 bar), ethylene (0.05 bar). Graphs A-C) show regions at which spectral features were expected on the basis of prior literature.[2] All spectra were taken for a laser power of 600 mW with an exposure time of 7.5 s for 10 frames. Spectra have been offset vertically for clarity. Single point data, attributed to stray electronic signals, have been removed as part of data processing. All spectra were collected with a 532 nm excitation wavelength.

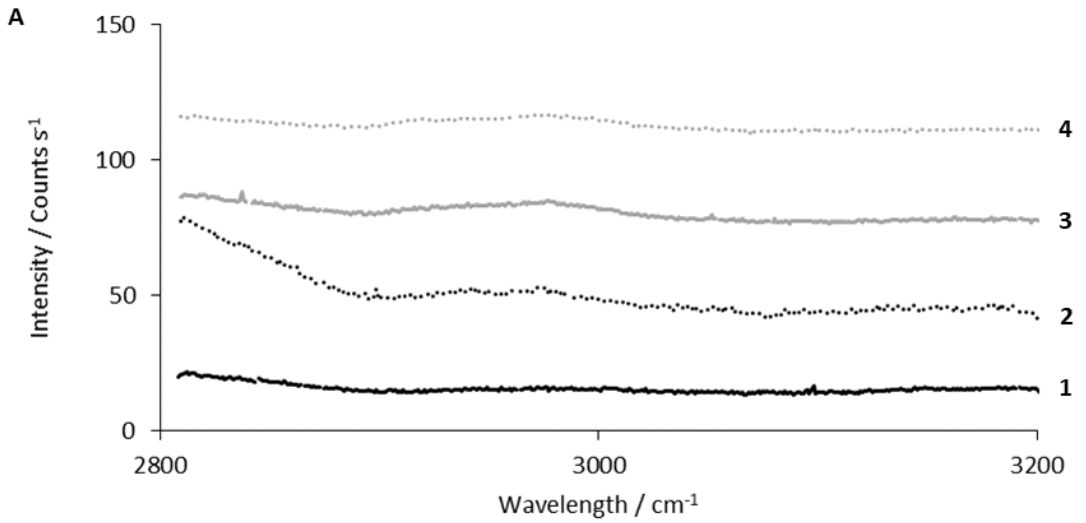

Figure 5.5. TIR Raman spectra of platinum/PVP nps LB deposited on a silica hemisphere and plasma cleaned for 2 min. Spectra were taken after replacement of the metal tubing, used to supply gas flow to the system, to nylon took place, as well as the addition of a zeolite adsorbent fitted to the hydrogen gas supply in order to remove any possible contamination. Figures 5.4 A-B and 5.5 A were taken with the following gas flow conditions 1- with no gas flow, 2- with helium (0.82 bar) flowing through the cell, 3- with a mixture containing helium (0.82 bar), and hydrogen (0.13 bar) flowing through the cell, 4- with a mixture containing helium (0.82 bar), hydrogen (0.13 bar), ethylene (0.05 bar). Graphs A-C) show regions at which spectral features were expected on the basis of prior literature.[2] All spectra were taken for a laser power of 600 mW with an exposure time of 7.5 s for 10 frames. Spectra have been offset vertically for clarity. Single point data, attributed to stray electronic signals, have been removed as part of data processing. All spectra were collected with a 532 nm excitation wavelength.

5.2. Raman setup, alignment and testing

Development of our own TIR Raman setup specialised to the needs of studies using nanoparticle catalysts was a major goal for the project. Components were chosen, with the help of results described earlier on pre-existing Raman setups, to tailor the system to be optimal for the systems being studied. Firstly, the purpose built setup is advantageous on a practical level in that the cell and gas delivery setup can be permanently located in an allocated space within the optical table – which proved more stable and allowed alignments to be better maintained between experiments. Secondly, in terms of spectroscopy, the purpose built setup employs a higher wavelength laser (660 nm *vs.* 532 nm), which was expected to reduce fluorescence from certain samples studied. Figure 5.6 shows a schematic of the setup. The CCD (Charge-Coupled Device) was also designed to work with the 660 nm laser, so that a low drop off in sensitivity is seen at the higher wavelengths that will result from Stokes scattering of the higher wavelength excitation light. The edge filters were chosen to allow frequencies as low as 150 cm^{-1} to eventually be detected (with some further/future work on polarisation dependant alignments), which could allow detection of copper(II) oxide

and silver(II) oxide with bands typically seen at 298, 347, and 591 cm^{-1} for copper(II) oxide, and 410 cm^{-1} for silver(II) oxide respectively.[3,4] This section describes the development of this new setup, firstly in terms of repetition of the most promising results obtained so far and a comparison between the two systems, followed by a further attempt at *in situ* detection under catalytic conditions.

A procedure for the alignment of the system (shown in Figure 5.6) was developed in the following way. Firstly, a torch was shone from the position of the CCD and spectrograph, going in the opposite direction to the Raman scattered light in the system when under normal operation. This was focussed to a focal point at the sample location. The light from the illuminator (I) was then adjusted using the illuminator lens so that the focal point matched that for the scattered light path (effectively the analytical focal point at which the sample would be probed). This illuminator enables accurate positioning of the sample and the laser beam at the analytical focal point once the CCD is reinstalled. Then, the laser was aligned working sequentially from the laser through to the sample. All alignments took place using low laser powers by placing an optical density (OD) filter in front of the laser source. Firstly, the beam expansion was checked to give the same 1 cm value at both short and long distances from the beam expander. Mirror M3 was then used to point and steer the beam, ensuring that the beam went through the centre of the polariser (P1) and the shutter (S). The beam is then aligned onto the sample at the analytical focal point identified using the illuminator as above, and monitored by the camera. This is done using mirror M4 and lenses L3 and L4, with one focusing in the x and the other in the y direction. The amount by which the mirror can be adjusted and the laser still visible in the camera through the objective is used to give an idea of the laser spot size (with a larger laser spot likely to need more variation). Once the laser spot is correctly aligned upon the centre of the sample the position can be subtly varied (using L3 and L4) in order to maximise the signal. Polarisers were also adjusted to maximise the signal empirically.

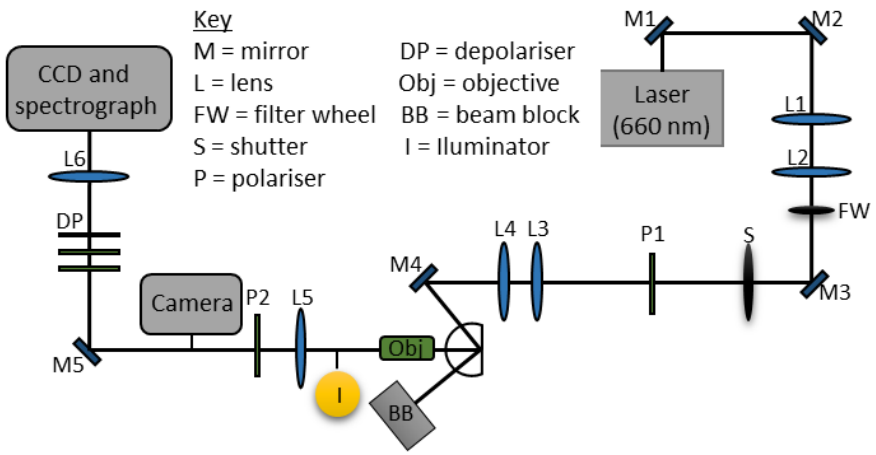

Figure 5.6. Schematic for setup of TIR Raman spectroscopic system purpose built for the in situ studies of nanoparticle catalysts.

5.2.1. White light and neon lamp calibrations

Firstly neon lamp calibrations were then undertaken in order to allow for calibration of wavelength. The spectrograph contained a choice of three gratings optimised for different ranges and resolutions. The two gratings known as "grating 2" (600 l/mm 750 nm blaze) and "grating 3" (1200 l/mm 600 nm blaze) were calibrated and used subsequently, as shown in Figure 5.7 A and 5.7 B for gratings 2 and 3 respectively.[5] The neon lamp was placed in front of the spectrograph (near the point marked camera in Figure 5.6). Calibrations of 5.5 and 4.5 cm^{-1} were made (*i.e.* actual value = measured value + 5.0, or 4.5 cm^{-1} respectively) for the setup when used with grating 2 and 3, respectively.

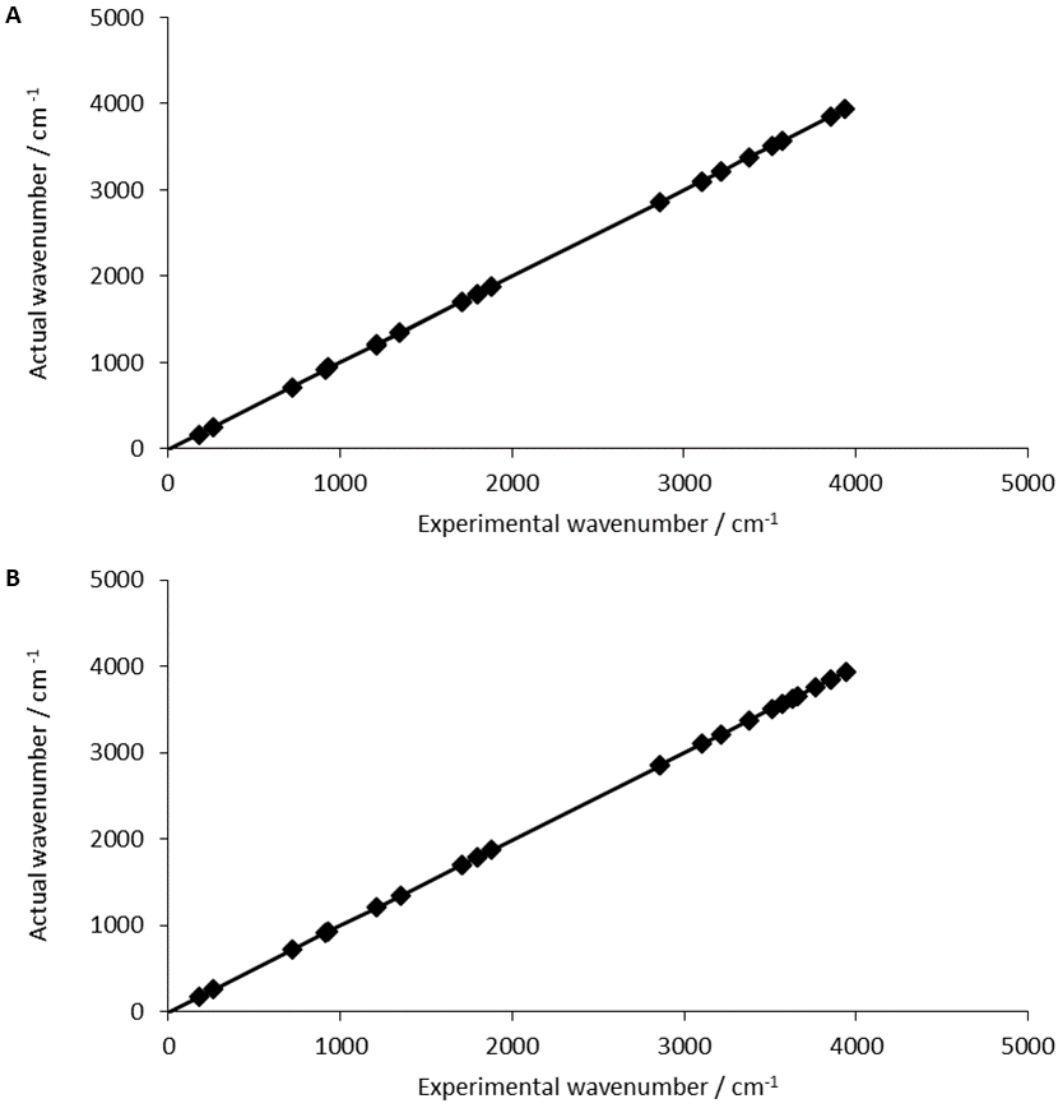

Figure 5.7. Neon lamp calibrations against a literature standard,[5] allowing correction of wavenumbers for the following gratings resulting in the corrections given A) grating 2, 5.5 cm^{-1} needed to be added to the experimental wavenumber and B) grating 3 where 4.5 cm^{-1} needed to be added to the experimental wavenumber.

White light calibrations were then undertaken to allow for a correction factor to be made to the spectra taken, in order to account for the variation in intensity as a function of wavelength in the collection system (everything from the objective lens to the CCD that could have chromatic sensitivity differences). This correction factor from these calibrations allows the shape of the spectra to be corrected. Where misalignments still occurred a mathematical fit would then be used to bring these correctly shaped spectra in line with each other. In order to achieve this the filament lamp was placed after the second polarizer (P2 in Figure 5.6). It should be noted that while a better location would be the sample spot this was logistically less straightforward because of the gas cell, and data sheets indicated that the objective lens and L5 should both exhibit minimal chromatic aberration. A reciprocal plot of

the white light spectra against the number of the data point is given, and allowed for fitting of a polynomial trend line providing a correction factor. Typical spectra taken before and after this calibration had been applied are shown in Figure 5.8. The inset shows the slight offset that has subsequently been aligned by a mathematical fit in the overlapping region to bring the two regions into alignment – as can be seen this is a small correction on the scale the spectra are presented.

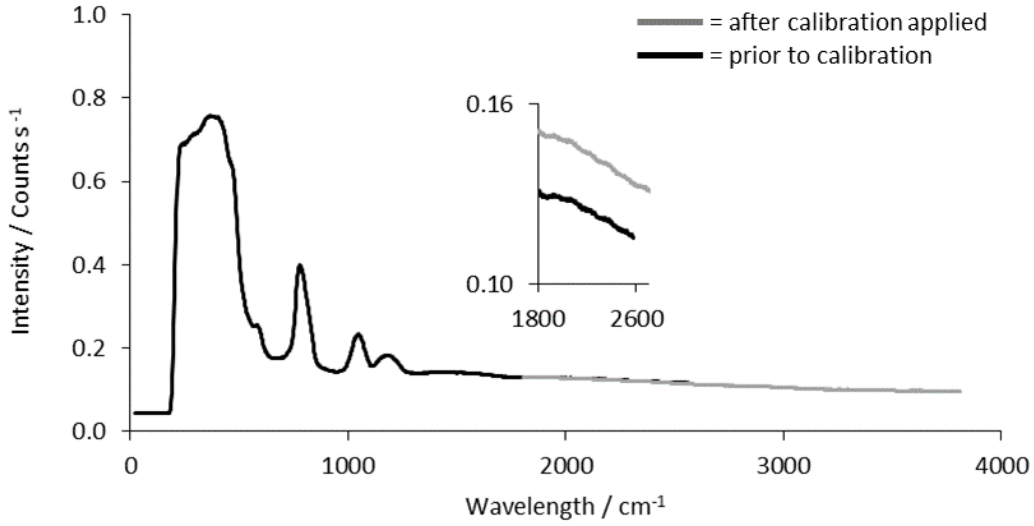

Figure 5.8. Typical TIR Raman spectra to show data before (in black) and after (in grey) white light calibrations have been applied. For the inset data has been magnified and offset vertically for clarity.

5.3. TIR Raman spectroscopic investigations using System 3

TIR Raman investigations undertaken on a purpose designed system are described within this section. Work within this section was conducted collaboratively with an undergraduate Erasmus project student (Patrick Ober, PO).

5.3.1. Reference spectra: Bulk spectra of capping agents

In order to aid spectral assignment, bulk spectra were recorded for a variety of capping agents (Figure 5.9). The spectra were recorded by placing the sample materials in a capillary tube. Capping agents of interest to this study, such as oleylamine or octadecylamine, were comprised of long aliphatic chains. Bands seen at 1500, 2900 cm^{-1} were assigned to CH deformation stretches, and CH_2 valence stretches respectively in the aliphatic chain. [6] Full assignment of oleic acid and oleylamine capping agents can be found in Chapter 3, Tables 3.6, and 3.7 respectively.

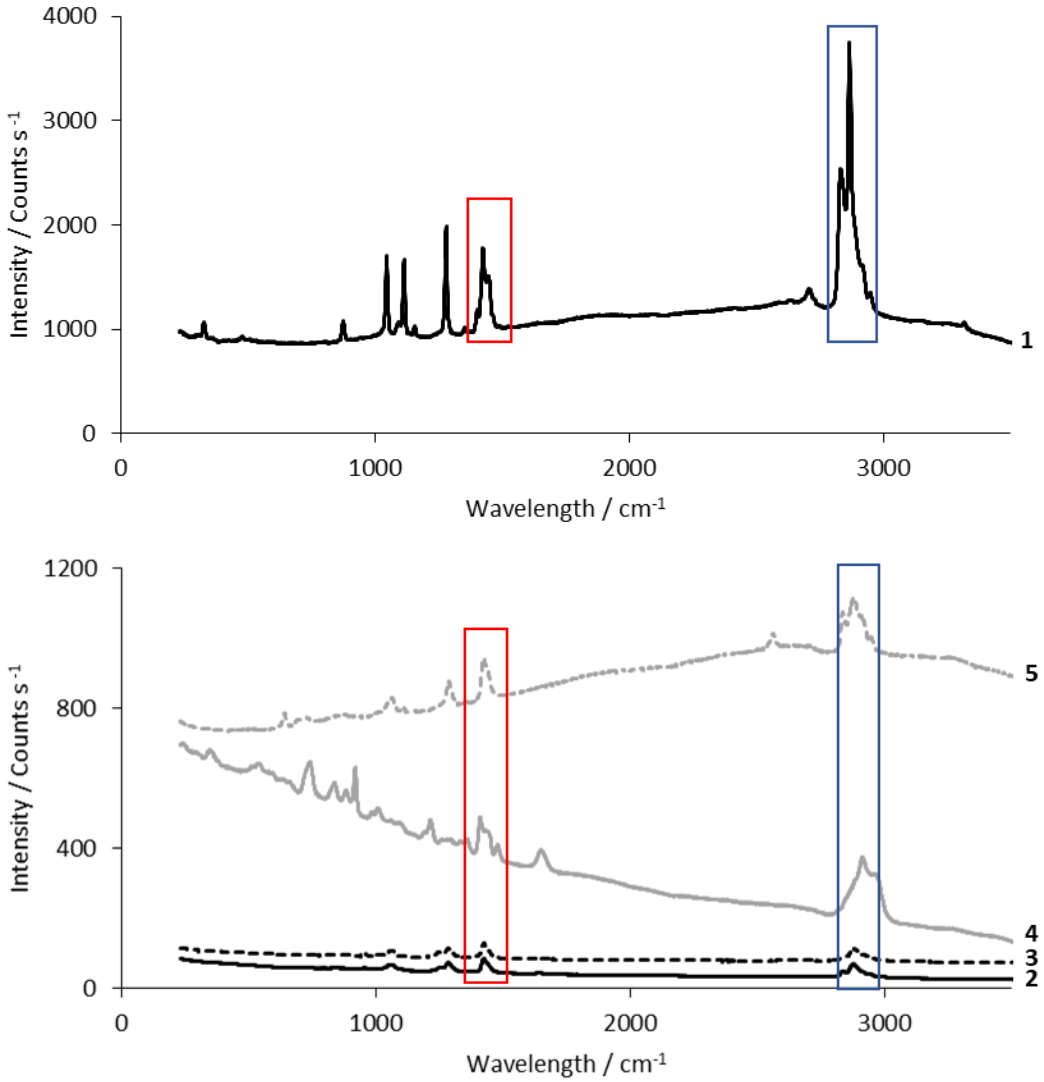

Figure 5.9 Bulk Raman spectra of capping agents 1- octadecylamine (5 s), 2- oleylamine (10 s), 3- oleic acid (10 s), 4- polyvinylpyrrolidone (5 s), and 5- dodecanethiol (5 s). All spectra were taken using grating 3 with a slit width of 100 µm. With key spectral features centred around 1500, and 2900 cm^{-1} marked by red and blue rectangles respectively. Spectra have been offset vertically for clarity. All spectra were obtained by placing the sample in a capillary tube using a laser power of 200 mW (set at the laser, with most of the power likely to reach the sample) for 10 frames. The exposure time per frame is indicated in brackets.

5.3.1.1. Comparison of bulk and drop cast spectra: dodecanethiol

TIR Raman spectra were taken for dodecanethiol capping agent deposited upon a silica hemisphere using the drop casting method (Figure 5.10, with drop casting described in Section 2.2.4.4.2). This spectrum was recorded in order to further understand the differences in features, such as intensity and frequency, between bulk and surface deposited capping agents. Such changes might be expected, for intensity and frequency, due to differences in near surface concentration resulting from preferential orientation and potential surface interaction on binding. Expected vibrational modes of dodecanethiol and the silica substrate

from the literature are given in Table 5.1 and Table 5.2, respectively. Assignments of the bulk spectrum obtained above (Figure 5.9) are given in Table 5.3, and that for the clean silica hemisphere is given in Table 5.4. The clean silica hemisphere was assigned in order to allow for the bands for the deposited material to be attributed above the clean silica hemisphere. On going from the bulk spectrum to the spectrum of dodecanethiol deposited on the silica hemisphere only four bands are reproduced, and for each a significant reduction in intensity is seen. No significant shift in wavelength was seen for the bands centred at approximately 1290, 2880, and 1425 cm^{-1} assigned to CH_2 wag, CH_2 ν-asym, and unassigned respectively. The unassigned band centred at approximately 3290 cm^{-1} for the bulk was not seen in the drop cast spectra.

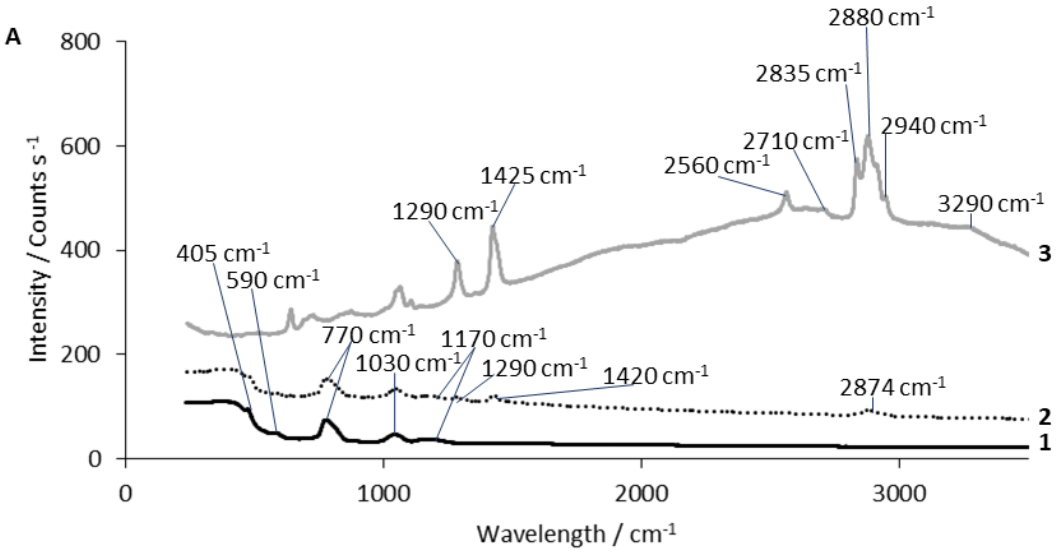

Figure 5.10 TIR Raman spectra taken for the following samples for 1- a clean silica hemisphere, 2- dodecanethiol drop cast onto silica hemisphere, 3- bulk spectra of dodecanethiol within a capillary tube. Spectra 1, and 2 were taken for a laser power of 600 mW with an exposure time of 20 s for 50 frames. Spectrum 3 was taken at a laser power of 200 mW with an exposure time of 5 s for 10 frames. All spectra were taken using grating 3 with a slit width of 100 µm. Spectra have been offset vertically for clarity.

Table 5.1. Literature values for expected Raman stretching frequencies for dodecanethiol.[6–17] *Where sym=symmetrical, asym=asymmetrical, v=vibration, wagg=wagg.*

Vibrational mode	Wavelength / cm^{-1}
CH_2 wagg	1295, 1326
S-H v	2575
CH_2 v-sym	2848, 2857, 2911, 2923
CH_2 v-asym	2882, 2891
CH_3 c	2873, 2956, 2962

Table 5.2. Literature values for expected Raman stretching frequencies for silica (quartz).[18–20] *Where asym=asymmetrical, and v=vibration.*

Vibrational mode	Wavelength / cm^{-1}
Si-Si v	275, 460, 505
Si-O fragments v	667, 949
Si-O-Si v-asym	1100
Si-O v	1230

Table 5.3. Assignment of Raman stretching frequencies for bulk dodecanethiol spectra. Where sym=symmetrical, asym=asymmetrical, v=vibration, wagg=wagg.

Vibrational mode	Wavelength / cm^{-1}
CH_2 wagg	1290
S-H v	2560
CH_2 v-sym	2835, 2940
CH_3 v-sym	2940
CH_2 v-asym	2880
unassigned	1425, 2710,3290

Table 5.4. Assignment of Raman stretching frequencies for clean silica hemisphere spectra. Where asym=asymmetrical, and v=vibration.

Vibrational mode	Wavelength / cm^{-1}
Si-Si v	405, 590
Si-O fragments v	770
Si-O-Si v-asym	1030
Si-O v	1170

5.3.2. Sensing nanoparticles: *ex situ*

Having shown the ability to detect the dodecanethiol capping agent in both the bulk form, using conventional Raman spectroscopy, and drop cast upon a silica hemisphere using TIR Raman spectroscopy, the study was extended to include the detection of monolayer concentrations of nanoparticles. Monolayer samples were required to give particles near enough to the silica/air interface to be within the TIR probing distance and to ensure, for *in situ* experiments, good contact between the gas phase and the nanoparticles (as no nanoparticles are buried under other layers of material). An explanation of the fundamentals, and theory behind this approach can be found in Section 2.1.5.4. The nanoparticles chosen for study were being used for other side projects within this and other work within the group.

5.3.2.1. Transmission electron microscopy (TEM) imaging and particle size analysis of cobalt nanoparticle system

TEM imaging and particle size distributions for cobalt/oleic acid nanoparticles (cobalt/OAc nps) is given in Figure 5.11 and shows spherical nanoparticles with a tight size distribution centred around 9 nm. Platinum/OAm nps, silver/copper/oleylamine nanoparticles (silver/copper/OAm nps), copper/oleylamine nanoparticles (copper/OAm nps) were made as per the methods in sections 2.2.1.2, 2.2.1.6, and 2.2.1.5 respectively but were not characterised.

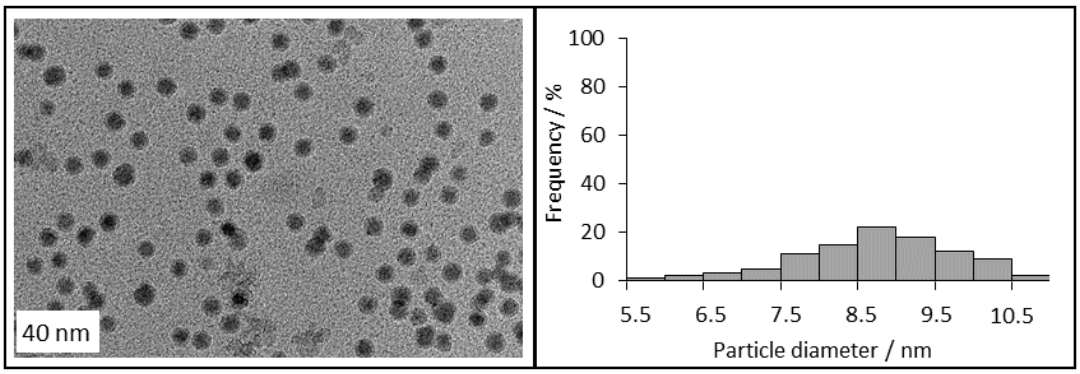

Figure 5.11. *(left) Typical TEM image of as synthesised cobalt/OAc nps (prepared as outlined in Section 2.2.1.3), (right) corresponding particle size distribution (9 ± 1 nm) obtained from multiple images of this sample.*

5.3.2.2. TIR Raman spectroscopic results

For deposition of a monolayer of silver/copper/OAm nps upon a silica hemisphere (Figure 5.12) replication of the bands from the oleylamine bulk Raman sample (875, 1120, 1345, 1445, and 2845 cm^{-1}) was seen, in both the 1500 and 2900 cm^{-1} regions for the monolayer sample. Literature assignments for oleylamine are given in Table 5.5 and the bands seen in Figure 5.12 are assigned fully in Table 5.6. Furthermore a small additional band not seen in the bulk oleylamine spectrum was also detected at 670 cm^{-1}. This could be due to interaction with the silica surface, or could be attributed to surface enhanced Raman scattering (SERS) effects. Although we do not expect to see SERS effects for these nanoparticles (particle size below 10 nm) it is possible that agglomeration has occurred within small regions of the sample. This could result in some irregular SERS activity increasing the intensity of bands that we cannot usually resolve.

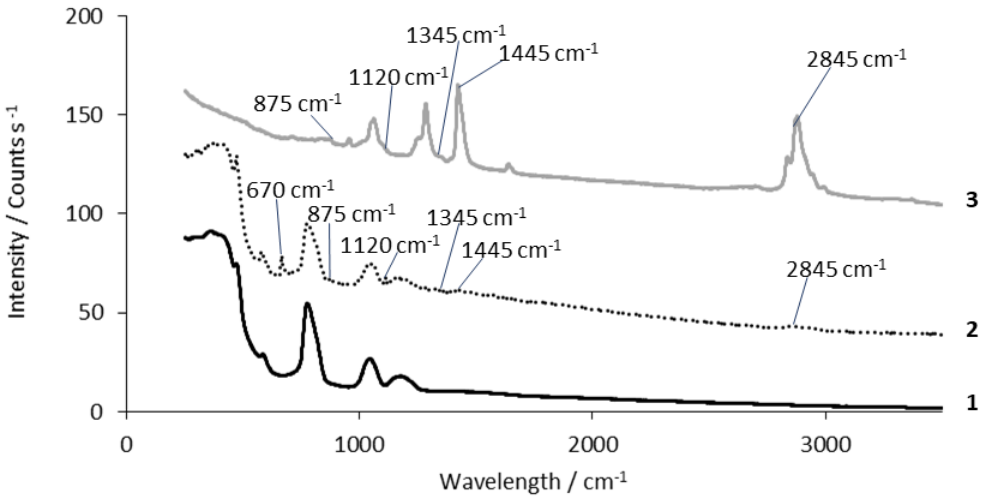

Figure 5.12. TIR Raman spectra taken for the following samples for 1- a clean silica hemisphere, 2- a monolayer of silver/copper/OAm nps (see Section 2.2.1.6) deposited using Langmuir Blodgett (LB) techniques onto a silica hemisphere (Section 2.2.5.9), 3- bulk spectra of oleylamine within a capillary tube. Spectra 1 and 2 were taken for a laser power of 600 mW with an exposure time of 20 s for 50 frames. Spectrum 3 was taken at a laser power of 200 mW with an exposure time of 10 s for 10 frames. All spectra were taken using grating 3 with a slit width of 100 µm. Spectra have been offset vertically for clarity.

Table 5.5. Literature table to show expected literature bands and assignments for capping agent oleylamine.[21,22] *Where sym=symmetrical, asym=asymmetrical, v=vibration.*

Literature vibrational mode	**Frequency / cm^{-1}**
C-C ν-sym	722
C-N ν-sym	1071
CH_3 ν-bend	1465
NH_2 ν-bend	1604, 795
C=C ν-sym	1647
C-H ν-asym and C-H ν-sym	2925, 2853
=C-H ν-sym	3004
N-H ν-sym	3300
NH_2 ν-asym and NH_2 ν-sym	3376, 3295

Table 5.6. Assignment of Raman stretching frequencies for oleylamine (OAm).[21,22] *Where sym=symmetrical, asym=asymmetrical, v=vibration, and unassigned-OAm bulk means the band could not be assigned but was seen in the bulk spectra of oleylamine.*

Assigned vibrational mode	**Frequency / cm^{-1}**
unassigned- OAm bulk	875,1345
C-N v-sym	1120
CH_3 v-bend	1445
C-H v-asym and C-H v-sym	2845

A variety of differing metals and capping agents were also tried and were deposited at a monolayer concentration upon a silica hemisphere (Figure 5.13). No bands were seen above the silica hemisphere background. This would further support that SERS activity contributes to the signal seen for in Figure 5.13 for the silver/copper/OAm nps. In order to determine that the lack of features was not due to decomposition of the nanoparticles under the laser beam data was taken at the beginning (the first 50 frames of data) and towards the end of the exposure (the last 50 frames). For the data (given in Figure 5A.3 within the Appendix) no significant variation was seen. This was except for small fluctuations which were accounted for by the changes in focus of the laser spot upon the hemisphere.

For the case of cobalt/OAc nps, the concentration deposited on the hemisphere was increased substantially (by using a drop casting method) to confirm that the nanoparticles did contain the expected organic molecules, and that they could be detected using TIR Raman spectroscopy. This approach allowed for detection of bands at 1440, 2755, 2870, and 2950 cm^{-1} as shown in the Figure 5.14. Based on the signal obtained for the drop cast layer, it was noted that if monolayer samples were to be detected then careful treatment of the data, to extract small signals expected (in the absence of SERS) is necessary.

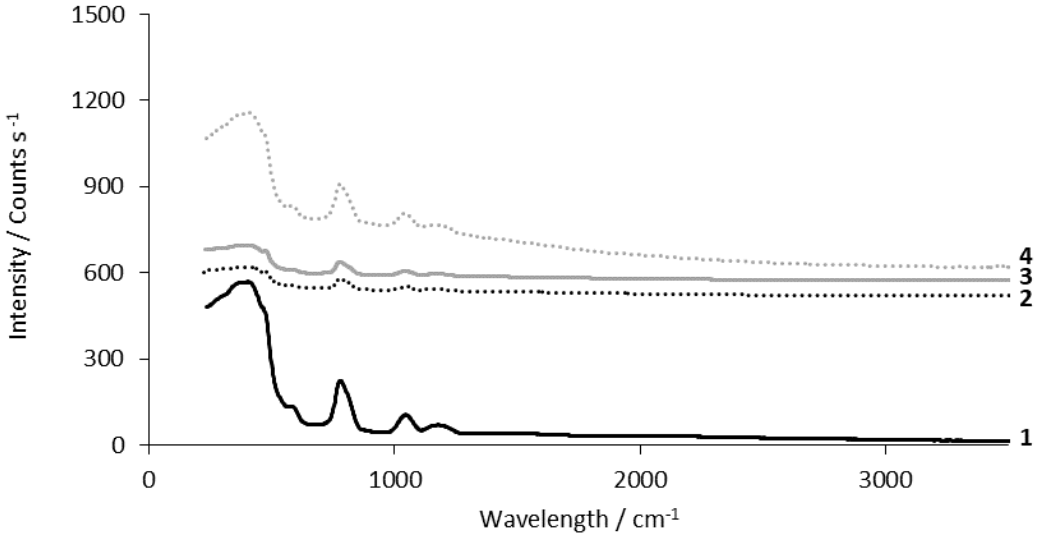

Figure 5.13. TIR Raman spectra taken for the following samples for 1- a clean silica hemisphere, and for the following nanoparticle samples deposited at a monolayer concentration upon a silica hemisphere using LB techniques (Section 2.2.5.9), 2- cobalt/OAc nps (see Section 2.2.1.3), 3- copper/OAm nps (Section 2.2.1.5), 4- platinum/OAm nps (Section 2.2.1.2). Spectra 1 and 2 were taken for a laser power of 600 mW with an exposure time of 20 s for 50 frames. Spectrum 3, and 4 were taken at a laser power of 600 mW with an exposure time of 20 s for 100 frames. All spectra were taken using grating 3 with a slit width of 100 µm. Spectra have been offset vertically for clarity.

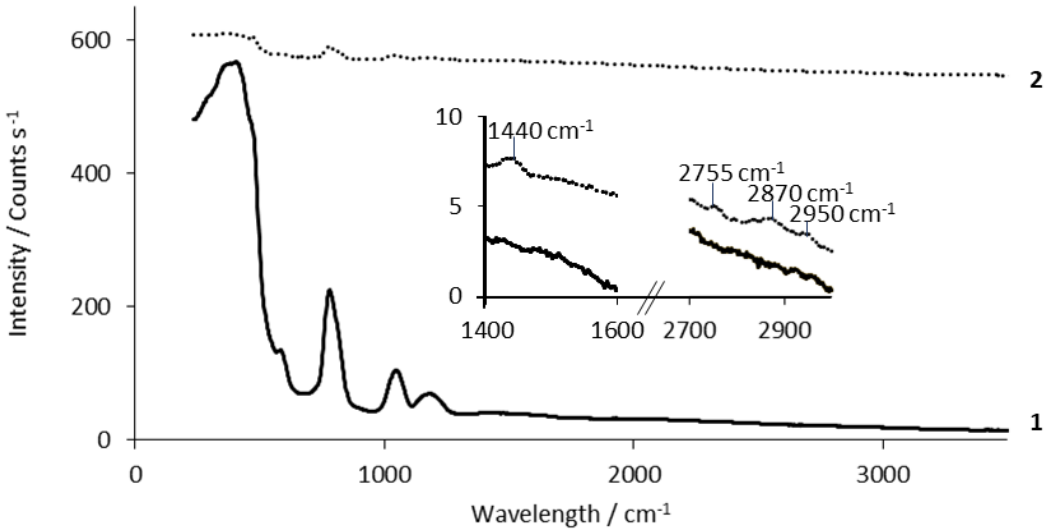

Figure 5.14. TIR Raman spectra taken for 1- a clean silica hemisphere, and 2- cobalt/OAc nps (see Section 2.2.1.3) drop cast upon a silica hemisphere (Section 2.2.4.4.2). Spectra have been offset vertically for clarity.

In order to identify small signals that were present, division spectra rather than subtracted background spectra were used. This allowed any changes to be identified more easily, as shown in Figure 5.15. As an aid to the eye a background has been fitted (grey) using a polynomial. Figure 5.15 shows only the region from 2000 cm^{-1} onwards, as initial examination of the whole 1200-3500 cm^{-1} region shows no other expected bands (as shown in the

Appendix Figure 5A.4). As can be seen one clear band centred at approximately 2910 cm^{-1} was present in all three spectra and was assigned to CH_2 stretches in the aliphatic chain.[6]

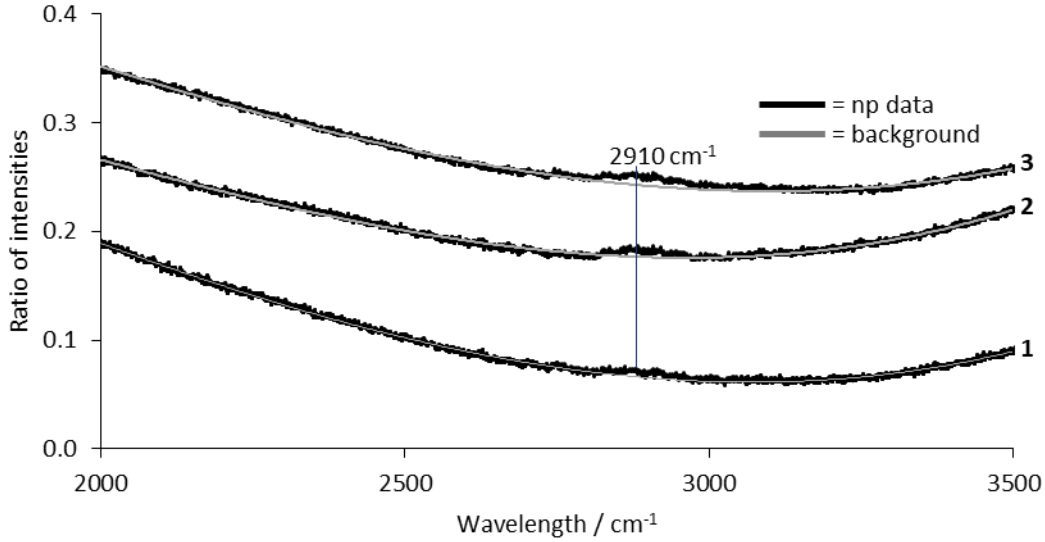

Figure 5.15. Division spectra for TIR Raman spectra taken in the region of 2000-3500 cm^{-1} for the following nanoparticle samples deposited at a monolayer concentration upon a silica hemisphere using LB techniques (Section 2.2.5.9) 1- cobalt/OAc nps (see Section 2.2.1.3), 2- copper/OAm nps (Section 2.2.1.5), 3- platinum/OAm nps (Section 2.2.1.2). All spectra have been divided by spectra of the clean silica hemisphere in order to allow for extraction of low intensity features. The following equations were used for each background 1) $y = 3E\text{-}11x^3 - 1E\text{-}07x^2 - 8E\text{-}05x + 0.5873$, 2) $y = 4E\text{-}11x^3 - 2E\text{-}07x^2 + 0.0002x + 0.3639$, 3) $y = 3E\text{-}11x^3 - 1E\text{-}07x^2 - 8E\text{-}05x + 0.5873$. Spectra 1 was taken for a laser power of 600 mW with an exposure time of 20 s for 50 frames. Spectrum 2, and 3 were taken at a laser power of 600 mW with an exposure time of 20 s for 100 frames. All spectra were taken using grating 3 with a slit width of 100 µm. Spectra have been offset vertically for clarity.

As part of the experimental setup two gratings were available. Grating 2 would be expected to provide a lower resolution but to allow for a higher spectral intensity. Grating 3 had been used for all experiments up unto this point due to the expected higher resolution. However, given the low intensity expected for any bands present both gratings were trialled and as well as accepting the lower resolution of grating 2, the slit width was increased to 200 µm. Spectra were recorded in this way for platinum/OAm nps deposited at a monolayer concentration on a silica hemisphere (Figure 5.16). The increased intensity seen when grating 2 was used resulted in a significant enhancement in the low intensity bands. Two bands at 2760, and 2870 cm^{-1} were seen assigned to C-H v-sym, and C-H v-asym CH_2 stretches in the aliphatic chain respectively (Table 5.5).[21,22] Therefore, despite the loss in resolution seen the use of grating 2 was preferential in this case due to the particularly low intensity of the bands present.

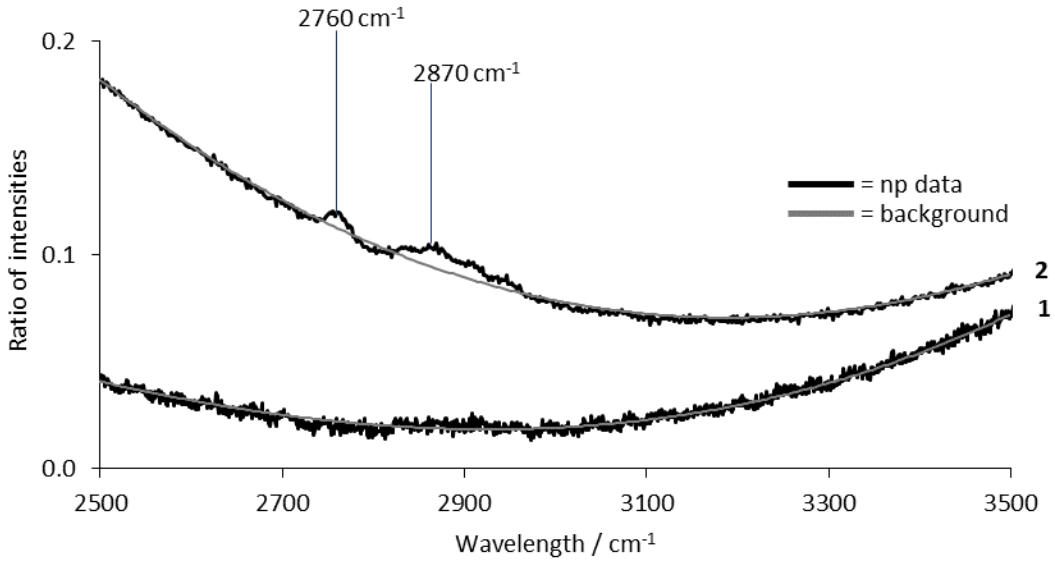

Figure 5.16. Division spectra for TIR Raman spectra taken for platinum/OAm np samples (Section 2.2.1.2) deposited at a monolayer concentration upon a silica hemisphere using LB techniques (Section 2.2.5.9) with the following gratings and slit widths 1- grating 3 slit width of 100 µm, and 2- grating 2 slit width of 200 µm. All spectra have been divided by spectra of the clean silica hemisphere in order to allow for extraction of low intensity features. The following equations were used for each background 1) y = -2E-11x3 + 4E-07x2 - 0.0021x + 3.0618, 2) $y = 4E\text{-}11x^3 - 2E\text{-}07x^2 + 0.0003x + 0.1704$. Both spectra were taken at a laser power of 600 mW with an exposure time of 20 s for 100 frames. Spectra have been offset vertically for clarity.

5.3.3. Plasma cleaning of platinum/OAm nps

As discussed in Chapter 3 removal of the organic capping agent is often desirable for catalytic and spectroscopic applications in order to give a clean surface. TIR Raman spectra of platinum/OAm nps before and after plasma cleaning (for 60 s) are given in Figure 5.17. A reduction in the intensity of both spectral features (centred at 2760, and 2870 cm^{-1}) was seen, indicating removal of the capping agent. Only a low intensity of both regions remained after plasma cleaning. This was expected to correlate to a negligible surface concentration of the species, or at the least the intensity of the bands was sufficiently low to provide the required clean surface for spectroscopy. Further plasma cleaning was not undertaken as unnecessarily long periods of plasma cleaning might be expected to induce agglomeration of the nanoparticles. The removal of these bands by plasma cleaning also acts as a confirmation of the assignment of these low intensity bands, above the spectral noise and background signal, to organic moieties on the surface that could be removed by the plasma cleaning process.

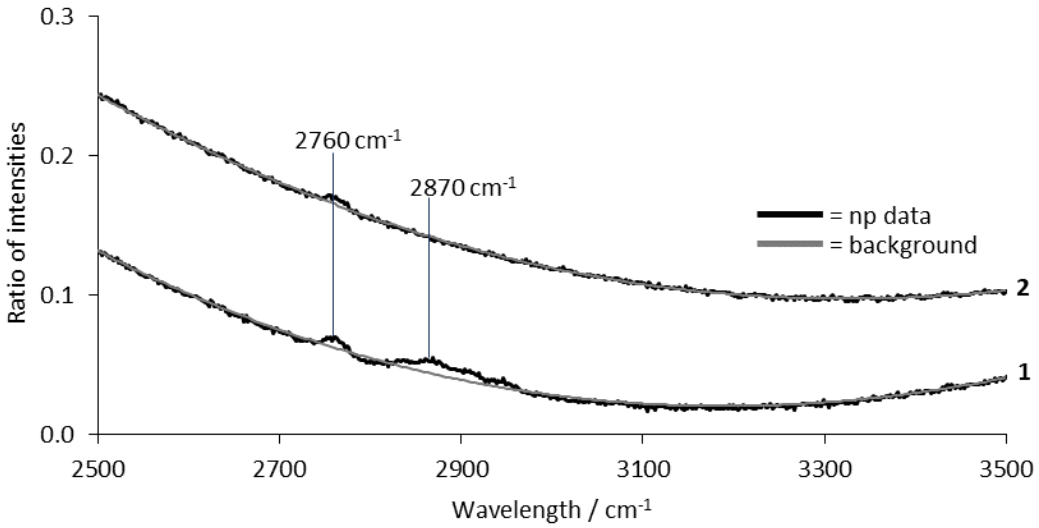

Figure 5.17. Division spectra for TIR Raman spectra taken for platinum/OAm np samples (Section 2.2.1.2) deposited at a monolayer concentration upon a silica hemisphere using LB techniques (Section 2.2.5.9) 1- prior to and, 2- after plasma cleaning for 60 s (Section 2.2.4.6). Both spectra were taken using grating 2 in order to maximise peak intensity. All spectra have been divided by spectra of the clean silica hemisphere in order to allow for extraction of low intensity features. The following equations were used for each background 1) $y = -4E\text{-}09x^3 + 6E\text{-}05x^2 - 0.245x + 338.74$, 2) $y = -3E\text{-}12x^4 + 3E\text{-}08x^3 - 9E\text{-}05x^2 + 0.0574x + 113.78$. Both spectra were taken at a laser power of 600 mW with an exposure time of 20 s for 100 frames. Spectra have been offset vertically for clarity.

5.3.4. Sensing nanoparticles: *in situ*

5.3.4.1 Blank hemispheres with gas feeds

In order to allow for backgrounding and referencing of the subsequent *in situ* spectra taken for the supported nanoparticle systems, spectra were taken for the clean silica hemisphere under the gas feed conditions used in the reaction (Figure 5.18). Firstly spectra were taken with no gas feed present, secondly with helium only, then with both helium and hydrogen, and finally with all three gases (helium, hydrogen and ethylene) present. Unprocessed spectra for all four gas feed conditions are shown in the Appendix (Figure 5A.5 A). No spectral features were identified. In order to extract any small features, division by the reference hemisphere took place as above. In this case the reference spectra was that of the clean silica hemisphere in the presence of inert gas helium (division spectra shown in the Appendix Figure 5A.5 B shows no differences exists between spectra for the clean hemisphere in the absence or presence of helium gas). Division spectra for the silica hemisphere in the presence of hydrogen and combined hydrogen and ethylene feeds both showed no significant features either. These results indicated that no interaction took place between the hemisphere and the ethylene gas phase. The spectra were also indicative of no purity issues being experienced for the gas phases used (as expected from the improvements implemented in Section 5.1).

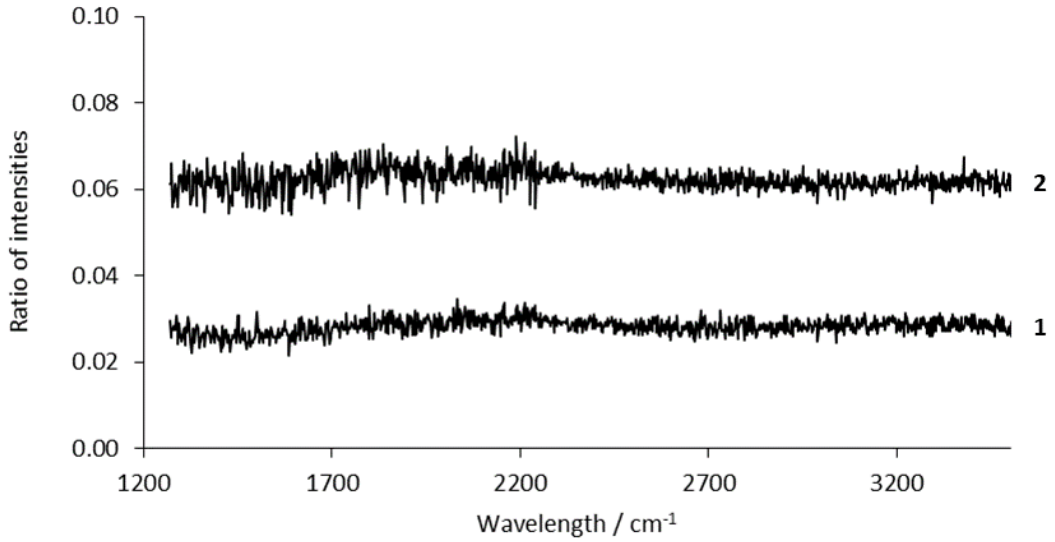

Figure 5.18. Difference spectra obtained from the TIR Raman spectra taken for a silica hemisphere in the presence of the following gas feeds 1- 0.83 bar of helium, and 0.13 bar of hydrogen, 2- 0.83 bar of helium, 0.13 bar of hydrogen and 0.04 bar of ethylene. Both spectra have been divided by spectra of the clean silica hemisphere in the presence of 0.83 bar of helium in order to allow for extraction of low intensity features. Both spectra were taken using grating 2 with a slit width of 200 µm in order to maximise peak intensity. Both spectra were taken at a laser power of 800 mW with an exposure time of 20 s for 50 frames. Spectra have been offset vertically for clarity.

5.3.4.2. In situ measurements for plasma cleaned platinum/OAm nps

TIR Raman spectra were obtained for platinum/OAm nps, deposited at a monolayer concentration on a clean silica hemisphere, with the deposited sample being plasma cleaned for 60 s prior to spectroscopy. Division spectra for all three gas flow conditions are shown in Figure 5.19. However, no bands were seen. In the present configuration this represents a limit on what could be achieved, and this is discussed in the future work section.

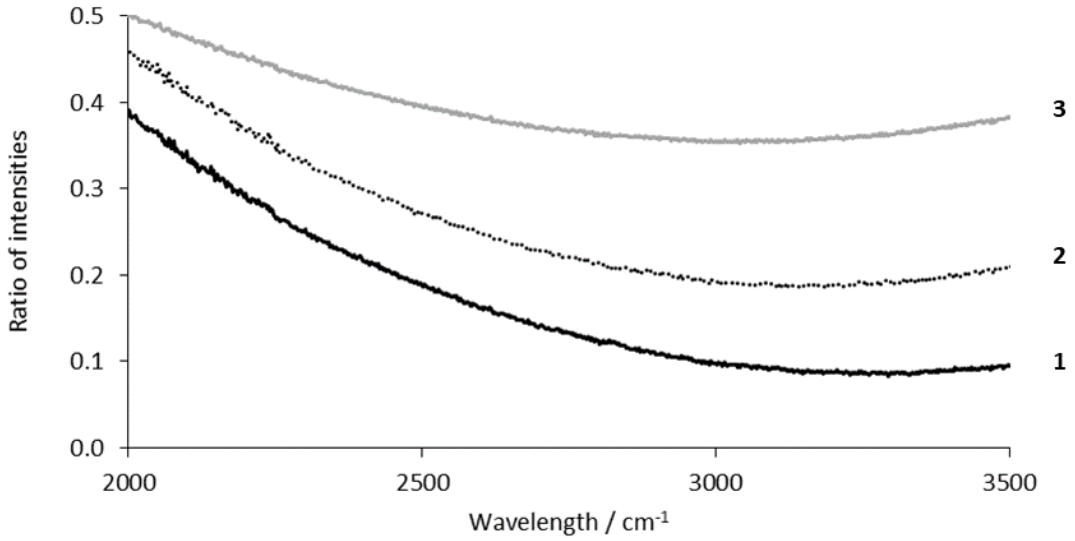

Figure 5.19. In situ TIR Raman spectra taken for a silica hemisphere deposited with a monolayer of platinum/OAm nps and plasma cleaned for 60 s in order to provide a clean surface in the presence of 1- 0.83 bar of helium, 2- 0.83 bar of helium, and 0.13 bar of hydrogen 3- 0.83 bar of helium, 0.13 bar of hydrogen, and 0.04 bar of ethylene. The spectra was divided by the spectra of the clean silica hemisphere in the presence of 0.83 bar of helium in order to allow for extraction of low intensity features. The spectra were taken using *grating 2 with a slit width of 200 µm in order to maximise peak intensity*. *Spectra were taken at a laser power of 800 mW with an exposure time of 20 s for 50 frames. Spectra have been offset vertically for clarity.*

5.4. Conclusions and future work

TIR Raman spectroscopy has been attempted for the *in situ* monitoring of ethylene hydrogenation over platinum nanoparticle catalysts and the use of an optimised spectrometer for such investigations has been explored both for observing capping agents on nanoparticles' surfaces and of the *in situ* investigation of ethylene hydrogenation.

A number of metal nanoparticle catalyst samples with several capping agents were examined using in the first instance TIR Raman spectroscopy of drop cast samples were compared to those obtained on the same system using bulk Raman spectroscopy of the capping agent molecules, indicating such species are on the nanoparticle surfaces. It was noted that copper and silver, although the nanoparticles themselves were small, appeared to exhibit significantly stronger than expected signals, likely due to a SERS enhancement. Deposition of a monolayer film on non-SERS active nanoparticles allowed the same features at 2760 and 2910 cm^{-1} to be seen, although only weakly. These could, as for samples in Chapter 3, be removed by plasma cleaning to leave a sample believed to be free for reaction and suitably free of competing signals for spectroscopy. While *in situ* studies of such monolayer deposited nanoparticles (platinum/OAm nps) were attempted for ethylene hydrogenation, this proved

to be out of the grasp of the sensitivity of the present instrument arrangement and so possible modifications are discussed in the future work section.

In conclusion for this system advancements have been made in reproducibly sensing monolayer concentration of nanoparticles deposited at the substrate surface. This has demonstrated the suitability of this technique towards the *in situ* study of heterogeneous catalytic reactions. However, at present further modifications of the system are required in order to allow for detection of such (predominantly gas phase) species under these *in situ* conditions.

5.5. Bibliography

(1) Cremer, P. S.; Su, X.; Shen, Y. R.; Somorjai, G. A. Ethylene Hydrogenation on Pt(111) Monitored in Situ at High Pressures Using Sum Frequency Generation. *J. Am. Chem. Soc.* **1996**, *118* (12), 2942–2949.

(2) Borodko, Y.; Habas, S. E.; Koebel, M.; Yang, P.; Frei, H.; Somorjai, G. A. Probing the Interaction of Poly(vinylpyrrolidone) with Platinum Nanocrystals by UV−Raman and FTIR. *J. Phys. Chem. B* **2006**, *110* (46), 23052–23059.

(3) Deng, Y.; Handoko, A. D.; Du, Y.; Xi, S.; Yeo, B. S. In Situ Raman Spectroscopy of Copper and Copper Oxide Surfaces during Electrochemical Oxygen Evolution Reaction: Identification of CuIII Oxides as Catalytically Active Species. *ACS Catal.* **2016**, *6* (4), 2473–2481.

(4) Pettinger, B.; Bao, X.; Wilcock, I.; Muhler, M.; Schlögl, R.; Ertl, G. Thermal Decomposition of Silver Oxide Monitored by Raman Spectroscopy: From AgO Units to Oxygen Atoms Chemisorbed on the Silver Surface. *Angew. Chem. Int. Ed. Engl.* **1994**, *33* (1), 85–86.

(5) Spectral calibration http://www.astrosurf.com/buil/us/spe2/hresol4.htm (accessed May 1, 2017).

(6) Bryant, M. A.; Pemberton, J. E. Surface Raman Scattering of Self-Assembled Monolayers Formed from 1-Alkanethiols at Silver [Electrodes]. *J. Am. Chem. Soc.* **1991**, *113* (10), 3629–3637.

(7) Snyder, R. G.; Strauss, H. L.; Elliger, C. A. Carbon-Hydrogen Stretching Modes and the Structure of N-Alkyl Chains. 1. Long, Disordered Chains. *J. Phys. Chem.* **1982**, *86* (26), 5145–5150.

(8) Yellin, N.; Levin, I. W. Cooperative Unit Size in the Gel-Liquid Crytalline Phase Transition of Dipalmitoyl Phosphatidylcholine-Water Multilayers: An Estimate from Raman Spectroscopy. *Biochim. Biophys. Acta BBA - Biomembr.* **1977**, *468* (3), 490–494.

(9) Compagnini, G.; Galati, C.; Pignataro, S. Distance Dependence of Surface Enhanced Raman Scattering Probed by Alkanethiol Self-Assembled Monolayers. *Phys. Chem. Chem. Phys.* **1999**, *1* (9), 2351–2353.

(10) Gaber, B. P.; Yager, P.; Peticolas, W. L. Interpretation of Biomembrane Structure by Raman Difference Spectroscopy. Nature of the Endothermic Transitions in Phosphatidylcholines. *Biophys. J.* **1978**, *21* (2), 161–176.

(11) Gaber, B. P.; Peticolas, W. L. On the Quantitative Interpretation of Biomembrane Structure by Raman Spectroscopy. *Biochim. Biophys. Acta BBA - Biomembr.* **1977**, *465* (2), 260–274.

(12) Spiker, R. C.; Levin, I. W. Phase Transitions of Phospholipid Single-Wall Vesicles and Multilayers. Measurement by Vibrational Raman Spectroscopic Frequency Differences. *Biochim. Biophys. Acta BBA - Biomembr.* **1976**, *433* (3), 457–468.

(13) Ha Joo, T.; Kim, K.; Soo Kim, M. Surface-Enhanced Raman Scattering of 1-Butanethiol in Silver Sol. *J. Mol. Struct.* **1987**, *158*, 265–274.

(14) Joo, T. H.; Kim, K.; Kim, M. S. Surface-Enhanced Raman Scattering (SERS) of 1-Propanethiol in Silver Sol. *J. Phys. Chem.* **1986**, *90* (22), 5816–5819.

(15) Schachtschneider, J. H.; Snyder, R. G. Vibrational Analysis of the N-paraffins—II. *Spectrochim. Acta* **1963**, *19* (1), 117–168.

(16) Hill, I. R.; Levin, I. W. Vibrational Spectra and Carbon–hydrogen Stretching Mode Assignments for a Series of N-alkyl Carboxylic Acids. *J. Chem. Phys.* **2008**.

(17) MacPhail, R. A.; Snyder, R. G.; Strauss, H. L. The Motional Collapse of the Methyl C–H Stretching Vibration Bands. *J. Chem. Phys.* **1982**, *77* (3), 1118–1137.

(18) Huber, K. P. *Constants of Diatomic Molecules*; Van Nostrand Reinhold: New York, 1979.

(19) Kopylov, V. B.; Pushkar', I. V. Chemical Features and Nature of Excited States in Silicon Oxides. *Russ. J. Gen. Chem.* **2006**, *76* (10), 1531–1532.

(20) Kopylov, V. B.; Aleksandrov, K. A.; Sergeev, E. V. Influence of Silicon Coordination Surrounding on the Chemical Structure of Oxides. *Russ. J. Gen. Chem.* **2007**, *77* (6), 1002–1003.

(21) Buck, M. R.; Biacchi, A. J.; Schaak, R. E. Insights into the Thermal Decomposition of Co(II) Oleate for the Shape-Controlled Synthesis of Wurtzite-Type CoO Nanocrystals. *Chem. Mater.* **2014**, *26* (3), 1492–1499.

(22) Shukla, N.; Liu, C.; Jones, P. M.; Weller, D. FTIR Study of Surfactant Bonding to FePt Nanoparticles. *J. Magn. Magn. Mater.* **2003**, *266* (1–2), 178–184.